Cell-Free Expressed Membraneless Organelles Inhibit Translation in Synthetic Cells

*Abbey O. Robinson[1], Jessica Lee[2], Anders Cameron[1], Christine D. Keating[2], Katarzyna P. Adamala[1]**

[1]Department of Genetics, Cell Biology and Development

University of Minnesota

420 SE Washington Ave.

Minneapolis, MN 55455, USA

[2]Department of Chemistry

The Pennsylvania State University

104 Chemistry Building

University Park, PA 16802, USA

Table of Contents Graphic

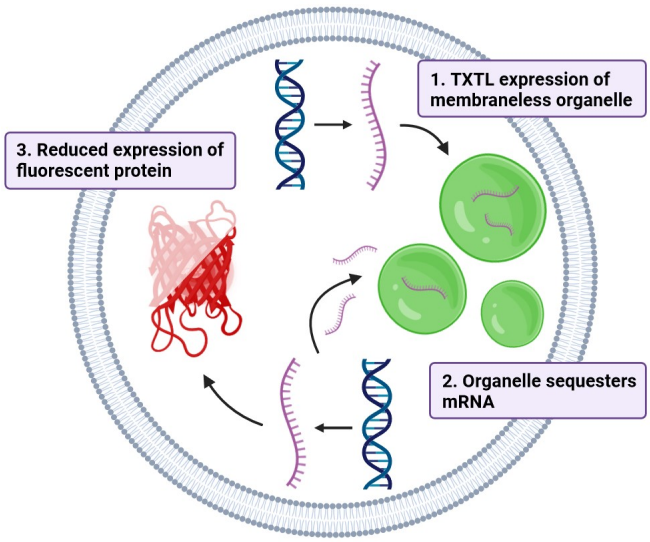

ABSTRACT: Compartments within living cells create specialized microenvironments, allowing for multiple reactions to be carried out simultaneously and efficiently. While some organelles are bound by a lipid bilayer, others are formed by liquid-liquid phase separation, such as P-granules and nucleoli. Synthetic minimal cells are widely used to study many natural processes, including organelle formation. In this work, synthetic cells expressing artificial membraneless organelles that inhibit translation are described. RGG-GFP-RGG, a phase-separating protein derived from *Caenorhabditis elegans* P-granules, is expressed by cell-free transcription and translation, forming artificial membraneless organelles that can sequester RNA and reduce protein expression in synthetic cells. The introduction of artificial membraneless organelles creates complex microenvironments within synthetic cell cytoplasm and functions as a tool to inhibit protein expression in synthetic cells. Engineering of compartments within synthetic cells furthers understanding of evolution and function of natural organelles and facilitates the creation of more complex and multifaceted synthetic life-like systems.

KEYWORDS: Synthetic biology, synthetic cells, cell-free expression, membraneless organelles, coacervates, translation

INTRODUCTION

The appearance of discrete intracellular compartments was critical for the evolution of eukaryotes. On average, eukaryotic cells are larger and functionally more complex than prokaryotic cells. This complexity can be attributed to the existence of the nucleus, as well as other compartments and organelles. The self-assembly of and spatiotemporal organization provided by intracellular compartments facilitates simultaneous and concatenate cell-processes that are unattainable in simpler organisms[1].

A key goal in bottom-up synthetic biology is to build artificial cells that mimic the functions and organization of living cells to create complex programmable bioreactors for foundational research and many practical applications[2]. To achieve this goal, there have been numerous efforts to build organelle-like compartments within synthetic cells to increase the complexity of synthetic cells and to better model and understand intracellular environments in natural cells. These efforts include engineering proto-organelles based on natural endosymbionts[3–6], oligolamellar vesicles[7,8], and lipid sponge droplets[9]. Inspired by membraneless organelles present in living cells, there has also been work on engineering protein-rich liquid droplets called coacervates as membraneless organelles for artificial cells[10–14].

Membraneless organelles are cellular compartments that lack a lipid bilayer. They are formed by liquid-liquid phase separation (LLPS), a thermodynamic-driven event characterized by the de-mixing of liquid phases—in cells, usually a dense protein- and/or RNA-rich phase separates from more dilute components. Many of these membraneless condensates are formed by intrinsically

disordered proteins (IDPs): dynamic proteins that lack tertiary structure. IDPs are ubiquitous, with approximately 30% of human proteins containing intrinsically disordered regions[15,16]. Ribonucleoprotein (RNP) particles are a type of these intracellular condensates formed between RNA and RNA-binding proteins which create cellular structures such as P-granules, stress granules, and nucleoli[17–20]. While RNP particles have diverse functions, many are involved in RNA processing, degradation, and storage, thus exerting a level of control over gene expression[21,22].

LAF-1 is an RNA helicase found in *Caenorhabditis elegans* P-granules which contain an intrinsically disordered region called the RGG (arginine-glycine-glycine) domain. Previously, it was found that RGG domains are critical for phase separation of LAF-1, and that the RGG domains themselves undergo liquid-liquid phase separation[23]. The RGG domain has low sequence complexity and consists of multiple arginine-glycine-glycine repeats. RGG domains often occur in repeats and are conserved in many other phase separating proteins[24]. RGG domains are also known to bind RNA, including G-quadraplexes[22,25–27].

More recently, the RGG domain was isolated and engineered to function as a synthetic membraneless organelle for both living and artificial cells[28,29]. Engineering synthetic cells that mimic the complexity and organization of living cells is a key goal in synthetic biology. The creation of compartments within liposome-based synthetic cells, or, better yet, a synthetic cell that can create its own compartments through cell-free gene expression will allow for more orthogonal capabilities of these artificial cells.

Significant obstacles to creating membrane-bound organelles within synthetic cells include issues with fusion of outer and inner vesicles, regulating the permeability of organelle

membranes, and lipogenesis[30]. Thus, creation of artificial organelles that are membraneless is an attractive option. More specifically, a major goal in pursuit of creating robust synthetic cells is regulation of gene expression, and membraneless organelles are known to sequester RNA, thereby playing a role in protein expression[22]. RNA accumulation within coacervates has also been studied in the context of the origins of life[31].

Many biological tools for modulation of gene expression that exist in complex living organisms have not been reconstituted in synthetic cells[32]. And while bacterial lysate-based cell-free protein expression has been exhibited within coacervates, to the best of our knowledge there has yet to be an example of synthetic cells that are able to endogenously synthesize protein-based organelles[33–36]. Here, we report the creation of an artificial membraneless organelle that can be expressed cell-free inside of synthetic cells and can sequester RNA to inhibit protein expression (Figure 1). We find that RGG-GFP-RGG, a recombinant protein with two RGG domains flanking GFP, forms coacervates when expressed by *in vitro* transcription and translation (TXTL), both in solution and when encapsulated inside of liposomes[37–39]. We observe localization of fluorescently labeled RNA to cell-free expressed RGG-GFP-RGG. We also find that the presence of RGG-GFP-RGG in TXTL reactions expressing another plasmid-encoded fluorescent protein sequesters RNA produced during transcription and results in reduced expression of protein. Together, this work provides a framework for the creation of protein-based compartments within synthetic cells.

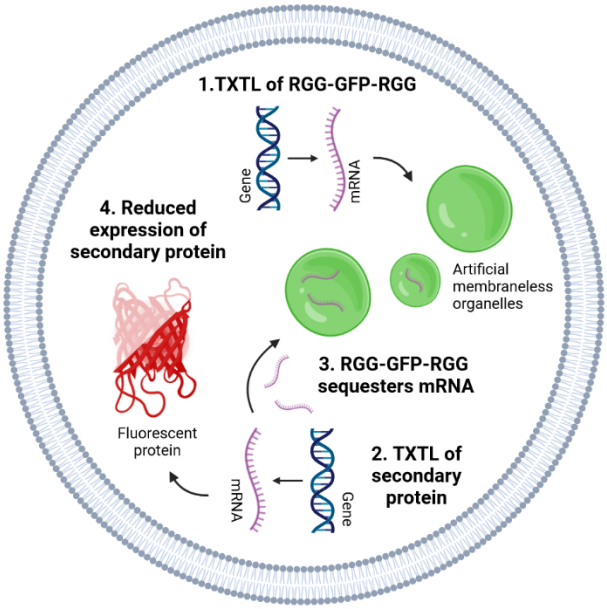

Figure 1. Schematic illustration of membraneless organelle expression and function in synthetic cell. A plasmid encoding for RGG-GFP-RGG, a phase separating protein, is expressed by TXTL to create coacervate droplets (membraneless organelle) inside of a liposome. When another plasmid—encoding for second fluorescent protein—is expressed by TXTL, RGG-GFP-RGG sequesters transcriptional mRNA, reducing expression and fluorescence of the secondary protein.

EXPERIMENTAL (MATERIALS AND METHODS)

Plasmid and oligonucleotide constructs: Plasmid information can be found in Table S1. Oligonucleotide sequences can be found in Table S2. pET_RGG-GFP-RGG and pET_RGG-RGG were gifts from Matthew Good, Daniel Hammer, and Benjamin Schuster (Addgene plasmids #124948, #124941). For transcription of RNA transcripts, corresponding DNA oligonucleotides were ordered from Integrated DNA Technologies (IDT). Cyanine5-labeled U(15) RNA (Cy5-U15) was custom purchased from Sigma-Aldrich.

Purification of RGG-GFP-RGG and RGG-RGG from E. coli: RGG-GFP-RGG and RGG-RGG were purified according to the methods previously described[5]. Plasmids were transformed in BL21(DE3) *E. coli* for protein expression. Cultures were grown in Terrific Broth (TB) media at 37°C while shaking at 250RPM until reaching OD600 = 0.6. Cultures were then induced with 1 mM isopropyl β-d-1-thiogalactopyranoside (IPTG) and incubated at 18°C, 225 RPM overnight for protein expression. The bacterial pellets were resuspended in high salt lysis buffer (500 mM NaCl, 20 mM Tris, 20 mM imidazole, 1mM PMSF, pH 7.5) and sonicated. To prevent phase separation, lysates were centrifuged at 15,000g for 30 minutes at 40C. Proteins were washed (500 mM NaCl, 20 mM Tris, 20 mM imidazole, pH 7.5), purified using Nickel NTA agarose beads (Catalog No. H-350-5, GoldBio), and eluted (500 mM NaCl, 20 mM Tris, 500 mM imidazole, pH 7.5). Finally, proteins were dialyzed overnight using a 7 or 10 kDa molecular weight cut-off Slide-A-Lyzer dialysis cassette (Catalog No. 66380, Thermo Scientific) in high salt buffer (500 mM NaCl and 20 mM Tris, pH 7.5) at 42°C to prevent phase separation. The dialyzed protein was aliquoted, flash frozen in liquid nitrogen, and stored at -80C.

Cell-free protein expression (TXTL) and quantification: Cell-free protein expression of RGG-GFP-RGG was carried out using a T7-based TXTL system adopted from the Noireaux lab and using methods described previously[40]. Cell extract was prepared from Rosetta2 *E. coli* by methods described previously[41]. TXTL reactions contain 10 nM DNA template, 12 mM magnesium glutamate, 140 mM potassium glutamate, 1 mM DTT, 1.5 μM T7 RNA polymerase, 0.4 U/μL Murine RNase Inhibitor, 1× energy mix, 1× amino acid mix, and cell free extract. The 10× energy mix is composed of the following: 500 mM HEPES, pH 8, 15 mM ATP, 15 mM GTP, 9 mM CTP, 9 mM UTP, 2 mg/mL E. coli tRNA, 0.68 mM Folinic Acid, 3.3 mM NAD, 2.6 mM Coenzyme-A, 15 mM Spermidine, 40 mM Sodium Oxalate, 7.5 mM cAMP, and 300 mM 3-PGA. The 10× amino

acid mix is composed of 17 mM of the following amino acids: alanine, arginine, asparagine, aspartic acid, cysteine, glutamic acid, glutamate, glycine, histidine, isoleucine, leucine, lysine, methionine, phenylalanine, proline, and serine.

For analysis of TXTL reactions using fluorescence, signal quantification was measured in 384-well plates (Catalog No. 09-761-85, Corning) using a microplate fluorometer (SpectraMax GeminiXS). Relative protein expression was estimated using western blot (Bio-Rad ChemiDoc).

Cell-free transcription: Short linear templates were used for expression of RNA transcripts. Sense and anti-sense oligos containing a T7Max promoter sequence and a short fragment (36 nucleotides) of the coding sequence for deGFP were synthesized (Integrated DNA Technologies) and annealed in a thermocycler. A master mix of transcription reagents was prepared on ice containing DNA template, 1X homemade NEB Buffer, 8 mM GTP, 4 mM A/C/UTP, 0.005X phosphatase 25 ng/μL, 1 μM T7 RNAP, and 0.4 U/μL Murine RNAse Inhibitor (Catalog No. M0314S, New England BioLabs). Reactions were incubated for 8 hours at 37°C in a thermocycler. RNA was purified using a Monarch RNA Cleanup Kit (500 μg) (Catalog No. T2050L, New England BioLabs) and concentration was measured using a NanoDrop ND-1000 UV-Vis Spectrophotometer (Thermo Scientific).

Turbidity assay: Phase properties of the protein were determined by measuring optical density (OD) at 600 nm using a microplate spectrophotometer (SpectraMax 340PC384). 100 μL TXTL reactions expressing RGG-GFP-RGG were prepared as well as a no DNA control TXTL reactions. Purified RGG-GFP-RGG in physiological buffer (150mM NaCl, 6mM Tris, pH 7.5) was also assayed. Samples were prepared in a clear 96-well microplate and readings were taken every 30 seconds as the instrument heated from ambient temperature (~25°C) to 40°C.

Liposome preparation and encapsulation: Thin films were prepared by dissolving 1mM 1-palmitoyl-2-oleoyl-sn-glycero-3-PC (POPC) and 1 mM cholesterol (Catalog No. 15102, Catalog No. 9003100, Cayman Chemical) in chloroform or dichloromethane in glass vials. Vials were left uncapped overnight in a fume hood to allow for the solvent to evaporate and thin films to form. Thin films were resuspended in mineral oil (Catalog No. 1632129, Bio-Rad) to create the lipid-in-oil solution. Internal contents were encapsulated in liposomes using water-in-oil emulsion method described previously[40]. For encapsulation of purified RGG-GFP-RGG, the protocol was carried out at room temperature. Nile Red was used to visualize liposome membranes (Catalog No. N1142, Thermo Scientific).

Electrophoretic mobility shift assay (EMSA): deGFP RNA binding to RGG-GFP-RGG was visualized by agarose gel electrophoresis. ~15 μg of purified deGFP RNA was added to 13.5 μM RGG-GFP-RGG in 150 mM NaCl and 6 μM Tris and loaded into a 1% agarose gel stained with 1X SYBR Safe DNA Gel Stain (Catalog No. S33102, Thermo Fisher). The mRNA was separated from the protein at 125 V for 45 minutes in 1X TAE buffer and gels were imaged (Aplegen Omega Lum G). The unbound RNA bands were quantified using Fiji.

Measuring mRNA abundance with quantitative reverse transcription PCR (RT-qPCR): TXTL and transcription reactions expressing deGFP were prepared in triplicate with either 8 μM RGG-RGG added or the corresponding volume of storage buffer. After incubation, TXTL and transcription reactions were centrifuged at 3200 g for 10 minutes to pellet RGG-RGG and bound mRNA. The supernatant was removed and treated with DpnI to degrade template plasmid DNA (Catalog No. R0176S, New England BioLabs Inc.). The mixture was incubated at 37˚C for 15 minutes (T100 Thermal Cycler, Bio-Rad). The enzyme and the expressed proteins were inactivated by adding

15mM EDTA (Catalog No. E9884, Sigma-Aldrich) at 75˚C for 10 minutes. The denatured proteins were pelleted through centrifugation at 3200 g for 2 minutes.

For the reverse transcription reaction, 4.5 µl of digested sample was added to 0.5µl of reverse primer (Integrated DNA Technologies), 0.5 µl of 10mM dNTP mix (Catalog No. CB4420-2, Denville Scientific), and 1 µl water. The reaction was incubated at 65˚C for 1 minute, then put on ice for at least 5 minutes. The digested sample was then added to 0.5 µl of Invitrogen SuperScript IV Reverse Transcriptase (Catalog No. 18090200, Thermo Fisher), 2 µl of 5x Superscript IV Buffer, 0.5 µl of 100mM DTT, and 0.5 µl of RNase Inhibitor, Murine (Catalog No. M0314S, New England BioLabs Inc.). The full reaction was then incubated at 52˚C for 10 minutes, and the reverse transcriptase was inactivated at 80˚C for 10 minutes.

The qPCR reaction was prepared in triplicate with 2 µl of the resultant cDNA from the reverse transcription, 2 µl of 10 µM forward and reverse qPCR primers (Integrated DNA Technologies), 11.25 µl OneTaq Hot Start 2X Master Mix with Standard Buffer (Catalog No. M0484, New England BioLabs Inc.), 1.25 µl Chai Green Dye 20X (Catalog No. R01200, Chai Bio), and 6.5 µl of nuclease-free water. The RT-qPCR was completed using CFX96 Touch Real-Time PCR Detection System (Bio-Rad) with the following thermocycling program: 1 cycle of 30 second denaturation at 94˚C, 30 cycles of 15 second denaturation at 94˚C, 15 second annealing at 54˚C, 1 minute extension at 68˚C, and 1 cycle of 5 minutes final extension at 68˚C. The amplification curves and Cq values were calculated through the CFX Maestro software. The averages across 3 biological and technical replicates were calculated, replacing non-detected values with 30 (the maximum cycle number).

Western blot analysis: Samples in 1x SDS-PAGE loading buffer were heated at 95 °C for 5 minutes and separated at 100 V for 1 h on 12% SDS-PAGE gels. Gels were transferred to a PVDF membrane at 100 V for 1 h in chilled buffer (25 mM Tris, 192 mM glycine, 10% methanol). The membrane was blocked in 5% nonfat milk in TBST for 1 h, followed by incubation with primary mouse anti-His antibodies (Catalog No. 652505, BioLegend) overnight. The membrane was rinsed three time with TBST followed by three 10 min washes in TBST. Secondary HRP goat anti-mouse antibodies (Catalog No. 405306, BioLegend) were added in 5% nonfat milk in TBST and incubated for 1 h, and washed as described previously. Blots were developed using SuperSignal Chemiluminescent Substrate (Catalog No. 34577, Thermo Scientific) and imaged using the ChemiDoc MP Imaging System (BioRad) running Image Lab version 5.2.1. Western blots characterizing TXTL reactions show a band for T7 polymerase, a His-tagged enzyme that is used for cell-free expression.

Fluorescence microscopy: Fluorescence and brightfield images were taken using a Nikon Eclipse Ti microscope and confocal images were taken using a Leica TCS SP5 microscope. Image brightness, contrast, and channel color were adjusted and scale bars were added using Fiji (ImageJ).

RESULTS

1. Cell-free expression of RGG-GFP-RGG forms coacervates inside of liposomes

We first determined if a coacervate-forming protein could be expressed by *in vitro* transcription and translation (TXTL). RGG-GFP-RGG, an intrinsically disordered protein labeled with green fluorescent protein, was used for cell-free protein expression experiments. The RGG protein was chosen for its relatively heterogeneous amino acid sequence, compared to other coacervate-

forming proteins, as we speculated highly repetitive sequences may be less compatible with TXTL expression. RGG-GFP-RGG contains two RGG domains flanking GFP, allowing for quantitative fluorescence spectroscopy and microscopy. RGG-GFP-RGG demonstrates upper critical solution temperature (UCST) phase behavior, meaning that above the critical temperature the proteins are miscible in solution, and below the critical temperature form coacervates[28]. In physiological buffer (150mM NaCl, 6mM Tris, pH 7.5) the critical temperature of RGG-GFP-RGG is around 40°C[28]. RGG-GFP-RGG forms liquid-like, spherical droplets at ambient temperatures and is reversibly miscible upon heating and cooling[28]. Previously, phase separation by purified RGG-GFP-RGG was observed in cell-like structures formed by aqueous droplets in oil[28]. For control experiments, RGG-GFP-RGG was purified from *E. coli* according to previous methods and phase separation was observed (Figure 2a).

The pET_RGG-GFP-RGG-His plasmid was expressed by TXTL, and a microplate fluorometer was used to assay fluorescence intensity of the GFP-tagged RGG protein over the course of the TXTL reaction to confirm expression (Figure S1). deGFP, a truncated version of eGFP which has been optimized for cell free expression, was also expressed as a positive control[42]. From this kinetic assay, we observed increased fluorescence of RGG-GFP-RGG, similar to the deGFP positive control. We also confirmed successful expression of RGG-GFP-RGG by western blot (Figure S2). The concentration of RGG-GFP-RGG expressed in TXTL was estimated to be approximately 5 μM (Figure S2). Together, these two assays indicate the protein can be expressed by TXTL. Since coacervate formation is dependent on salt, pH, and protein concentration, we next confirmed that when expressed by TXTL, RGG-GFP-RGG still forms coacervates. We imaged the reactions on a fluorescence microscope and observed protein-rich droplets in TXTL reactions expressing RGG-GFP-RGG, but not deGFP (Figure 2b-c). RGG-

GFP-RGG droplets purified from *E. coli* and in physiological buffer are much larger than when expressed by TXTL, this is likely due to differences in protein concentration and buffer composition[16].

To characterize the temperature-dependent phase behavior of the TXTL-expressed protein, turbidity was measured at different temperatures using a microplate spectrophotometer (Figure 2d, Figure S3). A TXTL reaction expressing RGG-GFP-RGG was prepared and incubated for 8 hours, and the resultant reaction (approximately 5 μM RGG-GFP-RGG concentration) was assayed for temperature-dependent turbidity, along with a TXTL reaction with no DNA template and RGG-GFP-RGG purified from E. coli (13.5 μM RGG-GFP-RGG concentration) in physiological buffer. Absorbance readings at OD600 were taken as the plate reader warmed from ambient temperature (~25°C) to 40°C. It was previously reported that RGG-RGG, a protein containing two identical RGG domains to RGG-GFP-RGG but no GFP domain, in physiological buffer at 12 μM RGG domain concentration has a transition temperature around 40°C. In our assay, RGG-GFP-RGG had transition temperature around 35°C[28]. This lower transition temperature could be due to the presence of GFP, which does not phase separate under these conditions (Figure 2c, 2g). RGG-GFP-RGG expressed by TXTL had similar phase properties as the purified protein, with a critical temperature around 40°C, albeit the TXTL reaction was considerably more turbid compared to the no DNA control and purified RGG-GFP-RGG protein. This could be due to interaction of RGG-GFP-RGG with components present in the TXTL reaction mix. The phase behavior of RGG-GFP-RGG expressed by TXTL further suggests the protein is expressed and undergoes coacervation when expressed cell-free.

We wished to create a synthetic cell that is capable of producing its own microcompartments. To confirm the RGG-GFP-RGG protein forms coacervates when bound within a lipid membrane,

we encapsulated the purified protein in liposomes. RGG-GFP-RGG was encapsulated at 9 μM concentration in POPC/cholesterol liposomes using a water-in-oil emulsion method[40]. Phase separation of RGG-GFP-RGG was observed within the liposomes (Figure 2e, Figure S4).

To engineer the synthetic cells expressing RGG-GFP-RGG condensates, TXTL reactions expressing the RGG-GFP-RGG plasmid were prepared and encapsulated in POPC/cholesterol liposomes. Following encapsulation, the liposomes were incubated at 30˚C for expression and subsequently imaged using fluorescence microscopy. Fluorescent condensates were observed in the liposomes containing the RGG-GFP-RGG TXTL reaction (Figure 2f, Figure S4, Video S1), while none were observed in liposomes expressing deGFP (Figure 2g), showing that cell-free expression of RGG-GFP-RGG within liposomes results in the formation of condensates. Sufficient protein concentration of RGG-GFP-RGG was necessary for condensate formation within liposomes, which is varied due to the stochastic partitioning of the TXTL reaction mixture during encapsulation. The morphology of the condensates appears distinct from that of multilamellar and multivesicular vesicles; in the multilamellar vesicles, the internal liposomes have a lumen[43] (Figure S5).

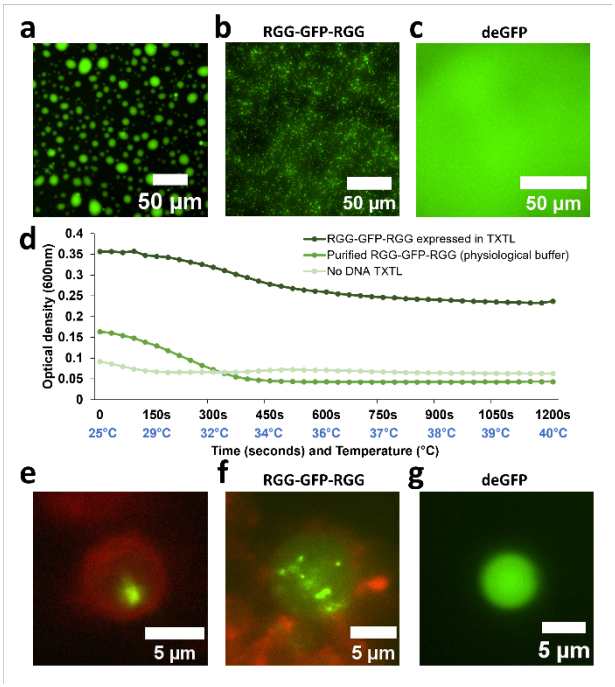

Figure 2. Phase separation of cell-free expressed RGG-GFP-RGG. a) RGG-GFP-RGG purified from *E. coli* (20 µM, in storage buffer). b-c) Phase separation of RGG-GFP-RGG expressed in TXTL reaction (b), compared to no phase separation observed in deGFP control (c). d) Turbidity assay depicts phase properties of RGG-GFP-RGG expressed by TXTL. OD600 is measured over time, with the temperature at each time point noted in blue. e) RGG-GFP-RGG purified from *E. coli* forms condensates (green) when encapsulated inside 1 mM POPC/1 mM cholesterol liposomes stained with Nile Red (red). f-g) RGG-GFP-RGG expressed from a plasmid in TXTL reaction forms condensates (f) when encapsulated inside 1 mM POPC/1 mM cholesterol liposomes; no condensates are observed in deGFP control (g).

2. Creating RNA-binding membraneless organelles in synthetic cells

After verifying we can create condensates within synthetic cells, we then sought to functionalize these microcompartments. Membraneless organelles are known to play a role in controlling gene

expression through mRNA regulation, and RGG-domains are known RNA binding domains, so we wished to exploit RNA-binding of the cell-free expressed RGG-GFP-RGG coacervates to create organelles capable of cell-wide translation inhibition within synthetic cells[22,24–26].

RNA binding to RGG domains is well known and has been characterized previously by electrophoretic motility shift assays (EMSA)[36,44,45]. To confirm binding of labeled RNA in our system, we used EMSA to observe interactions between RGG-GFP-RGG and RNA. We transcribed RNA from a short (36 nucleotide) fragment of the deGFP coding sequence (Table S2). Length and structure affect RNA binding to coacervates, and for these experiments we chose to use a sequence derived from GFP, a protein that is well expressed by TXTL, so mRNA should not contain any secondary structures inhibiting translation[46]. RNA encoding for a fragment of deGFP was transcribed, incubated with RGG-GFP-RGG, and ran on an agarose gel (Figure 3a). The gel was stained with 1% SYBR-Safe for visualization of RNA, however GFP-tagged RGG-GFP-RGG can also be visualized under blue light. The intensity of the band of deGFP RNA that migrated on the gel was quantified (Figure 3b). The unbound RNA in the sample with RGG-GFP-RGG present had a 27% decrease in intensity compared to the RNA-only control, indicating that RNA remained bound to RGG-GFP-RGG and did not migrate down the gel. Smearing was also noted in lanes with RGG-GFP-RGG, suggesting that bound nucleic acid carried over from purification.

Further, Cy5-labelled U15 RNA (Cy5-U15) was used to visualize RNA sequestration by RGG-GFP-RGG. Cy5-U15 was added to purified RGG-GFP-RGG and imaged, and clear localization of Cy5-U15 to RGG-GFP-RGG was observed (Fig 3c). Cy5-U15 and RGG-GFP-RGG were then encapsulated in POPC/cholesterol liposomes, where localization of Cy5-U15 RNA to the condensates was seen once again (Figure 3d). We then wished to confirm sequestration of Cy5-

U15 RNA by coacervates expressed in cell-free reactions. TXTL reactions expressing RGG-GFP-RGG were prepared, and the reaction and Cy5-U15 were encapsulated in liposomes and incubated. After expression, RGG-GFP-RGG condensates were visible in the liposomes, with Cy5-U15 localized to the condensates (Figure 3e). Cy5-U15 localization to deGFP expressed by TXTL was not observed (Figure S6, Figure S7). A slight change in position of the droplets is seen, due to the movement of the condensates within the liposome and the switching time of the microscope filter turret.

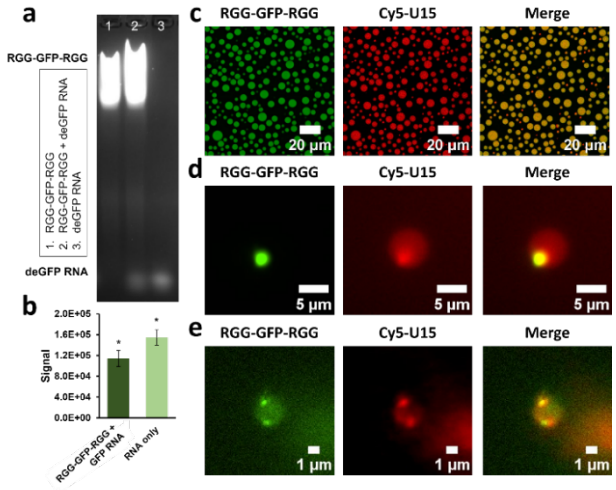

Figure 3. RNA sequestration by RGG-GFP-RGG membraneless organelles. a) RGG-GFP-RGG (13.5 µM) and deGFP RNA (~20 µg) on 1% agarose gel stained with SYBR-Safe. b) Gel quantification of migrated deGFP RNA bands in (a). Binding of RNA to RGG-GFP-RGG reduced intensity of migrated RNA band. Error bars signify SEM (n = 3) as determined by t-test, $*p < 0.05$. Confocal view of RGG-GFP-RGG coacervates binding Cy5-U15 RNA. d) RGG-GFP-RGG and Cy5-U15 encapsulated in POPC/cholesterol liposomes binds Cy5-U15. e) A TXTL reaction expressing RGG-GPF-RGG was encapsulated with Cy5-U15 in liposomes. Cy5-U15 localization to the RGG-GFP-RGG droplets is observed.

3. RNA sequestration by RGG-GFP-RGG condensates affects downstream protein expression

The presence of condensates containing RGG domains has been shown to bind RNA and reduce protein expression by cell-free expression systems[36]. Since the degree by which RNA or other molecules necessary for TXTL expression may be partitioned or sequestered by RGG-GFP-RGG, we first verified that other proteins can be expressed in the presence of the RGG-GFP-RGG coacervates without being totally inhibited[47]. TXTL reactions expressing deGFP were prepared, with the addition of increasing concentrations of purified RGG-GFP-RGG protein. The resultant expression of deGFP was then characterized by western blot (Figure 4a). The western blot showed that deGFP was expressed by TXTL in the presence of the IDP. Interestingly, there is an inverse relationship between the amount of RGG-GFP-RGG present and the level of deGFP expression: as more IDP is added to the reaction, deGFP expression decreases. Our hypothesis is that RGG-GFP-RGG binds transcriptional RNA during cell-free expression, resulting in lessened protein expression.

To confirm that RGG-GFP-RGG reduces protein expression by sequestering RNA, we used quantitative reverse transcription PCR (RT-qPCR) to quantify mRNA abundance in TXTL reactions when RGG protein is present (Fig 4b). TXTL reactions expressing deGFP were prepared in PCR tubes, not in vesicles, and non-fluorescent RGG-RGG was added. RGG-RGG contains the same RGG domains as RGG-GFP-RGG, but contains no GFP and was used instead of RGG-GFP-RGG to reduce potential artifacts from using the GFP-tagged protein during qPCR. Prior to RT, the samples were spun down to pellet the condensates and bound RNA and the supernatant containing free transcriptional mRNA was used for further reactions. Flourescence readings of GFP from the TXTL reactions were also taken (Figure 4c). Both free mRNA

abundance and fluorescence were depleted in TXTL reactions with RGG-RGG added, suggesting that RGG binds mRNA from transcription, thereby reducing the availability of mRNA to be translated into deGFP. Using the Cq values from Figure 4b to estimate the starting concentrations of template cDNA corresponding to the free mRNA (Starting template = $10^{((Cq - b)/m)}$ where m is the slope and b is the intercept calculated from the qPCR standard curve (Figure S8) of known DNA template concentrations), there was 2.3-times more template DNA in the positive control TXTL compared to the sample with RGG-RGG added. Similarly, the fluorescence signal of the deGFP positive control measured 2.5-times stronger than the reaction with RGG-RGG added, consistent with the depletion of RNA.

To see if this effect was seen when expressing RGG-GFP-RGG cell-free, we set up TXTLs with two plasmid templates, expressing both RGG-GFP-RGG and mCherry, another fluorescent protein, in one reaction (Figure 4). Our hypothesis was that the expressed RGG-GFP-RGG protein would phase separate to form model membraneless organelles that would in turn sequester transcriptional mRNA needed for mCherry expression, reducing mCherry fluorescence signal. This was indeed observed, with mCherry fluorescence signal decreased by 55% when expressed with RGG-GFP-RGG as compared to co-expression with deGFP (Figure 4e). It is also likely that RGG-GFP-RGG sequesters its own mRNA as well, possibly negatively regulating its own expression. While we did not explore this concept in this research, the autoinhibition provided by the RGG system may be of interest for future work. Of note, mCherry has a lower overall brightness compared to GFP resulting in lower average RFU values[48]. To confirm that the decrease in fluorescence was not due to fluorescence artifacts from the presence of the RGG-GFP-RGG droplets, protein expression was also measured by western blot and quantified (Figure 4d, Figure S9). The two-plasmid TXTL of RGG-GFP-RGG and mCherry showed decreased

mCherry band intensity on western blot compared to the positive control TXTL expressing both GFP and mCherry, indicating that mCherry expression was significantly hindered by the presence of RGG-GFP-RGG droplets. Together, this demonstrates that when co-expressed using TXTL, RGG-GFP-RGG membraneless organelles can suppress cell-free expression of another plasmid.

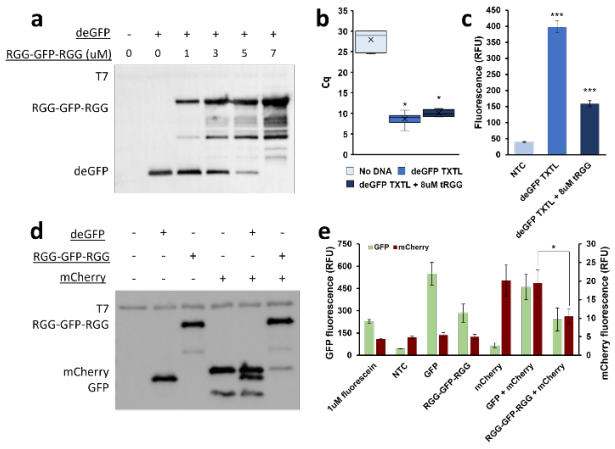

Figure 4. Sequestration of transcriptional mRNA by RGG proteins reduces protein expression in TXTL. a) TXTL reactions expressing deGFP were prepared and supplemented with increasing concentrations of RGG-GFP-RGG. RGG-GFP-RGG reduces deGFP expression in concentration dependent manner. Bands for T7 RNA polymerase are shown, a His-tagged enzyme included in the TXTL reaction mix. b) RT-qPCR was performed targeting deGFP in TXTL reactions with tRGG added. Prior to RT, reactions were spun down to remove tRGG and bound mRNA and the supernatant was taken for RT and subsequent qPCR. Reactions with tRGG present had elevated Cq values, indicating free mRNA abundance was reduced when tRGG was removed. Error bars signify SEM (separate TXTL reactions were considered biological replicates (n=3); each biological replicate underwent qPCR in triplicate (n=3)). Significance was determined by t-test, $*p < 0.05$. c) deGFP fluorescence in TXTL reactions with tRGG added was reduced, $***p <$

0.001. d-e) TXTL reactions expressing multiple plasmids were prepared and analyzed by western blot (d) and spectrofluorometer (e). Two-plasmid TXTL reactions expressing GFP and mCherry had fluorescence values slightly reduced compared to controls; TXTL reactions expressing both RGG-GFP-RGG and mCherry showed expected fluorescence values for RGG-GFP-RGG, while mCherry fluorescence was significantly reduced, $*p < 0.05$.

DISCUSSION

Membraneless organelles have garnered increased interest in recent years as we learn more about their functions in natural cells, including their role in regulation of protein expression. Cells respond to stress by remodeling their transcriptome through transcription and degradation of mRNA. Membraneless organelles like P-bodies and stress granules store mRNA, affecting mRNA localization, translation, and degradation[49,50]. We aimed to design a system where the compartments inside synthetic cells can bind RNAs at the genome-scale, providing a proof of concept that synthetic cells can regulate their own gene expression as membraneless organelles do in living cells.

The compatibility of cell-free expression platforms with coacervates has been previously reported[34–36]. While some have been successful compartments for cell-free protein expression, many of these biomolecular condensates have proven to be incompatible with cell-free systems[34]. Therefore, we looked to biology to select a condensate that would be both suitable for TXTL expression and likely to impact TXTL once it was produced in sufficient quantities to undergo phase separation. The RGG-GFP-RGG sequence used here can be expressed in living cells, and is known to bind RNA[28,36]. There are several factors that can influence the depletion or total loss of protein production by cell-free systems within coacervates, including reduced concentrations

or sequestering of critical components such as RNA polymerase or ribosomes in or out of the condensates. While these other factors may be occurring in our system, it is clear that RGG-GFP-RGG other RGG domain proteins bind RNA, resulting in reduced expression of secondary proteins[36].

CONCLUSION

Increasing the complexity of and creating versatile tools for synthetic cells is a major pursuit in synthetic biology. In this work, we demonstrated synthetic cells expressing the coacervate-forming protein RGG-GFP-RGG to function as artificial membraneless organelles. RGG-GFP-RGG was expressed by TXTL at sufficient quantities to promote phase separation inside of lipid vesicles. These artificial organelles were shown to sequester mRNA from TXTL reactions and reduce protein expression of plasmid-encoded proteins. Cellular organelles allow for certain biological processes to occur in a specialized environment, separated from the outside influences of the cell and these specialized compartments are critical for the numerous and complex functions of natural cells. Building organelles within synthetic cells not only increases the capabilities of synthetic cells, but also provides insight on spatiotemporal organization of natural biological cells and their origins.

ASSOCIATED CONTENT

Supporting Information. Supporting Information is available free of charge via the Internet at http://pubs.acs.org.

Supporting Information: Plasmid and oligo information and supplemental figures

Supplementary Video 1: Liposome encapsulating cell-free expressed RGG-GFP-RGG condensates

AUTHOR INFORMATION

Corresponding Author

* Katarzyna P. Adamala. kadamala@umn.edu.

Author Contributions

The manuscript was written through contributions of all authors. All authors have given approval to the final version of the manuscript.

ACKNOWLEDGMENTS

All authors were supported by the NSF award 1844313 RoL: RAISE: DESYN-C3: Engineering multi-compartmentalised synthetic minimal cells. AOR, AC and KPA were supported by the Alfred P. Sloan Foundation grant G-2022-19420, NSF award 2227578 Moving Millions of Droplets at Megahertz Speeds. AOR was supported by NIH Biotechnology Training Grant 5T32GM008347-29 and 5T32GM008347-30. Figures created with BioRender.com.

REFERENCES

(1) Mast, F. D.; Barlow, L. D.; Rachubinski, R. A.; Dacks, J. B. Evolutionary Mechanisms for Establishing Eukaryotic Cellular Complexity. *Trends Cell Biol* **2014**, *24* (7), 435–442. https://doi.org/10.1016/J.TCB.2014.02.003.

(2) Jia, H.; Schwille, P. Bottom-up Synthetic Biology: Reconstitution in Space and Time. *Curr Opin Biotechnol* **2019**, *60*, 179–187. https://doi.org/10.1016/J.COPBIO.2019.05.008.

(3) Trantidou, T.; Dekker, L.; Polizzi, K.; Ces, O.; Elani, Y. Functionalizing Cell-Mimetic Giant Vesicles with Encapsulated Bacterial Biosensors. *Interface Focus* **2018**, *8* (5). https://doi.org/10.1098/rsfs.2018.0024.

(4) Elani, Y.; Trantidou, T.; Wylie, D.; Dekker, L.; Polizzi, K.; Law, R. V.; Ces, O. Constructing Vesicle-Based Artificial Cells with Embedded Living Cells as Organelle-like Modules. *Scientific Reports 2018 8:1* **2018**, *8* (1), 1–8. https://doi.org/10.1038/s41598-018-22263-3.

(5) Agapakis, C. M.; Niederholtmeyer, H.; Noche, R. R.; Lieberman, T. D.; Megason, S. G.; Way, J. C.; Silver, P. A. Towards a Synthetic Chloroplast. *PLoS One* **2011**, *6* (4), e18877. https://doi.org/10.1371/JOURNAL.PONE.0018877.

(6) Holler, S.; Hanczyc, M. M. Autoselective Transport of Mammalian Cells with a Chemotactic Droplet. *Sci Rep* **2020**, *10* (1), 5525. https://doi.org/10.1038/s41598-020-62325-z.

(7) Lee, K. Y.; Park, S.-J.; Lee, K. A.; Kim, S.-H.; Kim, H.; Meroz, Y.; Mahadevan, L.; Jung, K.-H.; Ahn, T. K.; Parker, K. K.; Shin, K. Photosynthetic Artificial Organelles Sustain and Control ATP-Dependent Reactions in a Protocellular System. *Nature Biotechnology 2018 36:6* **2018**, *36* (6), 530–535. https://doi.org/10.1038/nbt.4140.

(8) Berhanu, S.; Ueda, T.; Kuruma, Y. Artificial Photosynthetic Cell Producing Energy for Protein Synthesis. *Nature Communications 2019 10:1* **2019**, *10* (1), 1–10. https://doi.org/10.1038/s41467-019-09147-4.

(9) Bhattacharya, A.; Niederholtmeyer, H.; Podolsky, K. A.; Bhattacharya, R.; Song, J.-J.; Brea, R. J.; Tsai, C.-H.; Sinha, S. K.; Devaraj, N. K. Lipid Sponge Droplets as Programmable Synthetic Organelles. *bioRxiv* **2020**, 2020.01.20.913350. https://doi.org/10.1101/2020.01.20.913350.

(10) Mason, A. F.; van Hest, J. C. M. Multifaceted Cell Mimicry in Coacervate-Based Synthetic Cells. *Emerg Top Life Sci* **2019**, *3* (5), 567–571. https://doi.org/10.1042/ETLS20190094.

(11) Mason, A. F.; Yewdall, N. A.; Welzen, P. L. W.; Shao, J.; Stevendaal, M. van; Hest, J. C. M. van; Williams, D. S.; Abdelmohsen, L. K. E. A. Mimicking Cellular Compartmentalization in a Hierarchical Protocell through Spontaneous Spatial Organization. *ACS Cent Sci* **2019**, *5* (8), 1360–1365. https://doi.org/10.1021/ACSCENTSCI.9B00345.

(12) Kato, S.; Garenne, D.; Noireaux, V.; Maeda, Y. T. Phase Separation and Protein Partitioning in Compartmentalized Cell-Free Expression Reactions. **2021**. https://doi.org/10.1021/acs.biomac.1c00546.

(13) Sokolova, E.; Spruijt, E.; Hansen, M. M. K.; Dubuc, E.; Groen, J.; Chokkalingam, V.; Piruska, A.; Heus, H. A.; Huck, W. T. S. Enhanced Transcription Rates in Membrane-Free Protocells Formed by Coacervation of Cell Lysate. *Proc Natl Acad Sci U S A* **2013**, *110* (29), 11692–11697. https://doi.org/10.1073/PNAS.1222321110/SUPPL_FILE/SM01.AVI.

(14) Donau, C.; Späth, F.; Sosson, M.; Kriebisch, B. A. K.; Schnitter, F.; Tena-Solsona, M.; Kang, H. S.; Salibi, E.; Sattler, M.; Mutschler, H.; Boekhoven, J. Active Coacervate Droplets as a Model for Membraneless Organelles and Protocells. *Nature Communications 2020 11:1* **2020**, *11* (1), 1–10. https://doi.org/10.1038/s41467-020-18815-9.

(15) Deiana, A.; Forcelloni, S.; Porrello, A.; Giansanti, A. Intrinsically Disordered Proteins and Structured Proteins with Intrinsically Disordered Regions Have Different Functional Roles in the Cell. *PLoS One* **2019**, *14* (8). https://doi.org/10.1371/JOURNAL.PONE.0217889.

(16) Brocca, S.; Grandori, R.; Longhi, S.; Uversky, V. Liquid–Liquid Phase Separation by Intrinsically Disordered Protein Regions of Viruses: Roles in Viral Life Cycle and Control of Virus–Host Interactions. *International Journal of Molecular Sciences 2020, Vol. 21, Page 9045* **2020**, *21* (23), 9045. https://doi.org/10.3390/IJMS21239045.

(17) Tauber, D.; Tauber, G.; Parker, R. Mechanisms and Regulation of RNA Condensation in RNP Granule Formation. *Trends Biochem Sci* **2020**, *45* (9), 764. https://doi.org/10.1016/J.TIBS.2020.05.002.

(18) Putnam, A.; Cassani, M.; Smith, J.; Seydoux, G. A Gel Phase Promotes Condensation of Liquid P Granules in Caenorhabditis Elegans Embryos. *Nature Structural & Molecular Biology 2019 26:3* **2019**, *26* (3), 220–226. https://doi.org/10.1038/s41594-019-0193-2.

(19) Hyman, A. A.; Weber, C. A.; Jülicher, F. Liquid-Liquid Phase Separation in Biology. *http://dx.doi.org/10.1146/annurev-cellbio-100913-013325* **2014**, *30*, 39–58. https://doi.org/10.1146/ANNUREV-CELLBIO-100913-013325.

(20) Lafontaine, D. L. J.; Riback, J. A.; Bascetin, R.; Brangwynne, C. P. The Nucleolus as a Multiphase Liquid Condensate. *Nature Reviews Molecular Cell Biology 2020 22:3* **2020**, *22* (3), 165–182. https://doi.org/10.1038/s41580-020-0272-6.

(21) Lee, C. Y. S.; Putnam, A.; Lu, T.; He, S.; Ouyang, J. P. T.; Seydoux, G. Recruitment of MRNAs to P Granules by Condensation with Intrinsically-Disordered Proteins. *Elife* **2020**, *9*. https://doi.org/10.7554/ELIFE.52896.

(22) Anderson, P.; Kedersha, N. RNA Granules. *Journal of Cell Biology* **2006**, *172* (6), 803–808. https://doi.org/10.1083/JCB.200512082.

(23) Elbaum-Garfinkle, S.; Kim, Y.; Szczepaniak, K.; Chen, C. C. H.; Eckmann, C. R.; Myong, S.; Brangwynne, C. P. The Disordered P Granule Protein LAF-1 Drives Phase Separation into Droplets with Tunable Viscosity and Dynamics. *Proc Natl Acad Sci U S A* **2015**, *112* (23), 7189–7194. https://doi.org/10.1073/PNAS.1504822112/SUPPL_FILE/PNAS.201504822SI.PDF.

(24) Chong, P. A.; Vernon, R. M.; Forman-Kay, J. D. RGG/RG Motif Regions in RNA Binding and Phase Separation. *J Mol Biol* **2018**, *430* (23), 4650–4665. https://doi.org/10.1016/J.JMB.2018.06.014.

(25) Kiledjian, M.; Dreyfuss, G. Primary Structure and Binding Activity of the HnRNP U Protein: Binding RNA through RGG Box. *EMBO Journal* **1992**, *11* (7), 2655–2664. https://doi.org/10.1002/J.1460-2075.1992.TB05331.X.

(26) Zanotti, K. J.; Lackey, P. E.; Evans, G. L.; Mihailescu, M. R. Thermodynamics of the Fragile X Mental Retardation Protein RGG Box Interactions with G Quartet Forming RNA. *Biochemistry* **2006**, *45* (27), 8319–8330. https://doi.org/10.1021/BI060209A/ASSET/IMAGES/MEDIUM/BI060209AN00001.GIF.

(27) Ohno, T.; Ouchida, M.; Lee, L.; Gatalica, Z.; Rao, V. N.; Reddy, E. S. P. The EWS Gene, Involved in Ewing Family of Tumors, Malignant Melanoma of Soft Parts and Desmoplastic Small Round Cell Tumors, Codes for an RNA Binding Protein with Novel Regulatory Domains. *Oncogene* **1994**, *9* (10), 3087–3097.

(28) Schuster, B. S.; Reed, E. H.; Parthasarathy, R.; Jahnke, C. N.; Caldwell, R. M.; Bermudez, J. G.; Ramage, H.; Good, M. C.; Hammer, D. A. Controllable Protein Phase Separation and Modular Recruitment to Form Responsive Membraneless Organelles. *Nat Commun* **2018**, *9* (1). https://doi.org/10.1038/S41467-018-05403-1.

(29) Caldwell, R. M.; Bermudez, J. G.; Thai, D.; Aonbangkhen, C.; Schuster, B. S.; Courtney, T.; Deiters, A.; Hammer, D. A.; Chenoweth, D. M.; Good, M. C. Optochemical Control of Protein Localization and Activity within Cell-like Compartments. *Biochemistry* **2018**, *57* (18), 2590–2596. https://doi.org/10.1021/ACS.BIOCHEM.8B00131/ASSET/IMAGES/LARGE/BI-2018-00131E_0004.JPEG.

(30) Roodbeen, R.; Van Hest, J. C. M. Synthetic Cells and Organelles: Compartmentalization Strategies. *BioEssays* **2009**, *31* (12), 1299–1308. https://doi.org/10.1002/BIES.200900106.

(31) Wollny, D.; Vernot, B.; Wang, J.; Hondele, M.; Safrastyan, A.; Aron, F.; Micheel, J.; He, Z.; Hyman, A.; Weis, K.; Camp, J. G.; Tang, T. Y. D.; Treutlein, B. Characterization of RNA Content in Individual Phase-Separated Coacervate Microdroplets. *Nature Communications 2022 13:1* **2022**, *13* (1), 1–9. https://doi.org/10.1038/s41467-022-30158-1.

(32) Gaut, N. J.; Adamala, K. P. Reconstituting Natural Cell Elements in Synthetic Cells. *Adv Biol* **2021**, *5* (3), 2000188. https://doi.org/10.1002/ADBI.202000188.

(33) Xu, C.; Martin, N.; Li, M.; Mann, S. Living Material Assembly of Bacteriogenic Protocells. *Nature 2022 609:7929* **2022**, *609* (7929), 1029–1037. https://doi.org/10.1038/s41586-022-05223-w.

(34) Schoenmakers, L. L. J.; Yewdall, N. A.; Lu, T.; André, A. A. M.; Nelissen, F. H. T.; Spruijt, E.; Huck, W. T. S. In Vitro Transcription–Translation in an Artificial Biomolecular Condensate. https://doi.org/10.1021/acssynbio.3c00069.

(35) Dora. Tang, T. Y.; Van Swaay, D.; DeMello, A.; Ross Anderson, J. L.; Mann, S. In Vitro Gene Expression within Membrane-Free Coacervate Protocells. *Chemical Communications* **2015**, *51* (57), 11429–11432. https://doi.org/10.1039/C5CC04220H.

(36) Simon, J. R.; Eghtesadi, S. A.; Dzuricky, M.; You, L.; Chilkoti, A. Engineered Ribonucleoprotein Granules Inhibit Translation in Protocells. *Mol Cell* **2019**, *75* (1), 66-75.e5. https://doi.org/10.1016/J.MOLCEL.2019.05.010.

(37) Shin, J.; Noireaux, V. An E. Coli Cell-Free Expression Toolbox: Application to Synthetic Gene Circuits and Artificial Cells. *ACS Synth Biol* **2012**, *1* (1), 29–41. https://doi.org/10.1021/SB200016S/SUPPL_FILE/SB200016S_SI_001.PDF.

(38) Garamella, J.; Marshall, R.; Rustad, M.; Noireaux, V. The All E. Coli TX-TL Toolbox 2.0: A Platform for Cell-Free Synthetic Biology. *ACS Synth Biol* **2016**, *5* (4), 344–355. https://doi.org/10.1021/ACSSYNBIO.5B00296/SUPPL_FILE/SB5B00296_SI_001.PDF.

(39) Garenne, D.; Thompson, S.; Brisson, A.; Khakimzhan, A.; Noireaux, V. The All-E. ColiTXTL Toolbox 3.0: New Capabilities of a Cell-Free Synthetic Biology Platform. *Synth Biol* **2021**, *6* (1). https://doi.org/10.1093/SYNBIO/YSAB017.

(40) Gaut, N. J.; Gomez-Garcia, J.; Heili, J. M.; Cash, B.; Han, Q.; Engelhart, A. E.; Adamala, K. P. Programmable Fusion and Differentiation of Synthetic Minimal Cells. *ACS Synth Biol* **2022**, *11* (2), 855–866. https://doi.org/10.1021/ACSSYNBIO.1C00519/ASSET/IMAGES/LARGE/SB1C00519_0004.JPEG.

(41) Gaut, N. J.; Gomez-Garcia, J.; Heili, J. M.; Cash, B.; Han, Q.; Engelhart, A. E.; Adamala, K. P. Programmable Fusion and Differentiation of Synthetic Minimal Cells. *ACS Synth Biol* **2022**, *11* (2), 855–866. https://doi.org/10.1021/ACSSYNBIO.1C00519/ASSET/IMAGES/LARGE/SB1C00519_0004.JPEG.

(42) Shin, J.; Noireaux, V. Efficient Cell-Free Expression with the Endogenous E. Coli RNA Polymerase and Sigma Factor 70. *J Biol Eng* **2010**, *4* (8), 8. https://doi.org/10.1186/1754-1611-4-8.

(43) Maja, L.; Željko, K.; Mateja, P. Sustainable Technologies for Liposome Preparation. *J Supercrit Fluids* **2020**, *165*, 104984. https://doi.org/10.1016/J.SUPFLU.2020.104984.

(44) Ozdilek, B. A.; Thompson, V. F.; Ahmed, N. S.; White, C. I.; Batey, R. T.; Schwartz, J. C. Intrinsically Disordered RGG/RG Domains Mediate Degenerate Specificity in RNA Binding. *Nucleic Acids Res* **2017**, *45* (13), 7984. https://doi.org/10.1093/NAR/GKX460.

(45) Chowdhury, M. N.; Jin, H. The RGG Motif Proteins: Interactions, Functions, and Regulations. *Wiley Interdiscip Rev RNA* **2022**, e1748. https://doi.org/10.1002/WRNA.1748.

(46) Sanchez-Burgos, I.; Espinosa, J. R.; Joseph, J. A.; Collepardo-Guevara, R. RNA Length Has a Non-Trivial Effect in the Stability of Biomolecular Condensates Formed by RNA-Binding Proteins. *PLoS Comput Biol* **2022**, *18* (2), e1009810. https://doi.org/10.1371/JOURNAL.PCBI.1009810.

(47) Parker, D. M.; Winkenbach, L. P.; Osborne Nishimura, E. It's Just a Phase: Exploring the Relationship Between MRNA, Biomolecular Condensates, and Translational Control. *Front Genet* **2022**, *13*, 1628. https://doi.org/10.3389/FGENE.2022.931220/BIBTEX.

(48) Cranfill, P. J.; Sell, B. R.; Baird, M. A.; Allen, J. R.; Lavagnino, Z.; De Gruiter, H. M.; Kremers, G. J.; Davidson, M. W.; Ustione, A.; Piston, D. W. Quantitative Assessment of Fluorescent Proteins. *Nat Methods* **2016**, *13* (7), 557. https://doi.org/10.1038/NMETH.3891.

(49) Protter, D. S. W.; Parker, R. Principles and Properties of Stress Granules. *Trends Cell Biol* **2016**, *26* (9), 668–679. https://doi.org/10.1016/J.TCB.2016.05.004.

(50) van Leeuwen, W.; Rabouille, C. Cellular Stress Leads to the Formation of Membraneless Stress Assemblies in Eukaryotic Cells. *Traffic* **2019**, *20* (9), 623–638. https://doi.org/10.1111/TRA.12669/.